Monthly Notices
of the
ROYAL ASTRONOMICAL SOCIETY

MNRAS **457,** 2415–2422 (2016) doi:10.1093/mnras/stw139

The low-mass end of the neutral gas mass and velocity width functions of galaxies in ΛCDM

C. Y. Yaryura,[1⋆] A. Helmi,[2] M. G. Abadi[1] and E. Starkenburg[3]

[1] *Instituto de Astronomía Teórica y Experimental (CONICET-UNC), Observatorio Astronómico de Córdoba, Laprida 854, X5000BGR, Córdoba, Argentina*
[2] *Kapteyn Astronomical Institute, University of Groningen, PO Box 800, NL-9700 AV Groningen, the Netherlands*
[3] *Leibniz-Institut für Astrophysik Potsdam (AIP), An der Sternwarte 16, D-14482, Potsdam, Germany*

Accepted 2016 January 13. Received 2015 December 18; in original form 2015 April 29

ABSTRACT

We use the high-resolution Aquarius cosmological dark matter simulations coupled to the semi-analytic model by Starkenburg et al. to study the H I content and velocity width properties of field galaxies at the low-mass end in the context of Λ cold dark matter (ΛCDM). We compare our predictions to the observed Arecibo Legacy Fast ALFA (ALFALFA) survey H I mass and velocity width functions, and find very good agreement without fine-tuning, when considering central galaxies. Furthermore, the properties of the dark matter haloes hosting galaxies, characterized by their peak velocity and circular velocity at two radial disc scalelengths overlap perfectly with the inferred values from observations. This suggests that our galaxies are placed in the right dark matter haloes, and consequently at face value, we do not find any discrepancy with the predictions from the ΛCDM model. Our analysis indicates that previous tensions, apparent when using abundance matching models, arise because this technique cannot be straightforwardly applied for objects with masses $M_{\rm vir} < 10^{10}{\rm M}_{\odot}$.

Key words: galaxies: dwarf – galaxies: haloes – galaxies: kinematics and dynamics – galaxies: luminosity function, mass function.

1 INTRODUCTION

The observed properties of our Universe on large scales are very well reproduced by the current standard Λ cold dark matter (ΛCDM) cosmological model (Komatsu et al. 2011). However, on small scales, the paradigm faces a number of challenges that could be related to inherent model flaws or due to our poor understanding and modelling of the physical processes that affect galaxies on these scales.

A well-known problem is the excess of low-mass dark matter haloes compared with the actual number of visible low-mass galaxies. This discrepancy is commonly known as the CDM overabundance problem or missing satellite problem (Klypin et al. 1999; Moore et al. 1999). One manifestation of this is evident in the faint end of neutral hydrogen (H I) mass functions (Papastergis et al. 2011) and in galaxy luminosity functions (LFs; Klypin et al. 2015). For example, dark matter-only simulations predict a slope for the mass function of $\alpha \sim -1.8$, which is in contrast to the significantly shallower slope $\alpha \sim -1.3$ exhibited for example by the H I mass function of galaxies in the Arecibo Legacy Fast ALFA (ALFALFA) survey (Martin et al. 2010).

The mass and LFs relate to properties of galaxies, but velocity functions are perhaps more revealing because they are connected to the internal properties of the host dark matter haloes. Papastergis et al. (2015) and Klypin et al. (2015) have recently drawn attention to the fact that the velocity function of dark matter haloes $\mathrm{d}N/\mathrm{d}\log V \sim V^{\alpha}$ has $\alpha \sim -3$, while observationally $\alpha \sim -1$ for galaxies with circular velocities smaller than $\sim$60 km s^{-1}.

Furthermore, it has been pointed out that CDM haloes hosting low-mass galaxies would be too concentrated in comparison to what can be inferred from observations, such as from rotation curves (Ferrero et al. 2012) or velocity dispersions at the half-light radii of dwarf galaxies (Boylan-Kolchin, Bullock & Kaplinghat 2012). This is known as the 'too big to fail problem' which has recently drawn a lot of attention in the literature.

We can classify the solutions to these problems in two types: those related to baryonic physics and those that propose changes in the nature of dark matter (see e.g. Kravtsov 2010, for a review). Among the many baryonic effects considered, we can mention photoheating during the reionization epoch (e.g. Barkana & Loeb 1999; Bullock, Kravtsov & Weinberg 2001; Shapiro, Iliev & Raga 2004) which results in a lower baryon fraction in low-mass haloes, the inability (or inefficiency) of H I cooling for haloes with virial temperature below 10^4 K (Haiman, Abel & Rees 2000), and stellar feedback (e.g. Dekel & Silk 1986; Mac Low & Ferrara 1999). The latter not only acts to lower the baryon fraction in low-mass galaxies, possibly preventing further star formation in the lowest mass systems, but may also modify the density profiles of dark matter haloes, making them less concentrated (Governato et al. 2012). On

⋆ E-mail: yaryura@oac.unc.edu.ar

the other hand, warm dark matter or self-interacting dark matter models, which effectively result in a suppression in the spectrum of fluctuations of the power on small scales, predict an important reduction in the number of small dark matter haloes, and possibly systems with lower central densities (e.g. Colín, Avila-Reese & Valenzuela 2000; Kamionkowski & Liddle 2000; Bode, Ostriker & Turok 2001; Kennedy et al. 2014; Polisensky & Ricotti 2014; Vogelsberger et al. 2014).

Fully cosmological numerical hydrodynamical simulations are just beginning to model reliably these low-mass scales, because of the difficulty in addressing simultaneously a large volume with high spatial resolution. Amongst the recent works that have discussed the issues highlighted above is Sawala et al. (2016) who have found that a combination of effects related to reionization and environment introduces strong biases in the haloes that host dwarf galaxies, and those that remain dark.

An alternative approach is to use semi-analytic (SA) models combined for example with a very high-resolution cosmological N-body simulation. For galaxies with neutral hydrogen mass $M_{\rm HI} \geq 10^8$ M$_\odot$, Obreschkow et al. (2013) show good agreement between the properties of gas-rich galaxies in the HI Parkes All-Sky Survey (HIPASS) survey to the predictions from an SA model coupled to the Millenium dark matter simulation (Springel et al. 2005). For lower masses, and using a different technique, namely abundance matching, Papastergis et al. (2015) argue that the ALFALFA survey should be observing a much larger number density of dwarf galaxies given the measured rotational velocities. Along similar lines, Garrison-Kimmel et al. (2014) predict there should be of the order of 1000 galaxies with stellar mass $M_* > 10^3$M$_\odot$ to be discovered within ∼3 Mpc from the Milky Way (MW). Furthermore, assuming a one-to-one relation between M_* and $M_{\rm HI}$ these authors predict 50 undiscovered gas-rich dwarf galaxies with $M_{\rm HI} > 10^5$M$_\odot$ within the local volume. However, care must be taken when applying abundance matching at the low-mass end (i.e. virial mass $M_{\rm vir} < 10^{10}$M$_\odot$), because this is a regime of strong stochasticity where galaxy formation may or may not take place in haloes of similar present-day mass depending on whether they were above or below a given threshold (e.g. for H I cooling) at higher redshift (see fig. 16 of Li, De Lucia & Helmi 2010). As we shall see in this paper (also in Sawala et al. 2016), for virial masses $M_{\rm vir} \sim 10^{9.5}$ M$_\odot$, only ∼50 per cent of the haloes are expected to host a galaxy. A simple abundance matching like-technique that only ranks haloes by mass around this mass scale will fail (Sawala et al. 2015).

Starkenburg et al. (2013) studied the properties of satellite galaxies around MW-like haloes combining an SA model with the Aquarius suite of cosmological simulations (Springel et al. 2008). This model reproduced well the LFs as well as e.g. star formation histories of these systems, and it was found that the 'too big to fail' problem could be solved by invoking a lower total mass for the MW of $\sim 8 \times 10^{11}$M$_\odot$ (Vera-Ciro et al. 2013). However, the model satellites had too high H I fractions, which was attributed to the lack of ram-pressure stripping of cold gas in the model once a galaxy becomes a satellite (see e.g. fig. 11 of Li et al. 2010, who use the same SA model but applied to a different cosmological simulation).

Motivated by the recent H I surveys such as HIPASS and ALFALFA that probe the lowest mass ends, and by the relative success in solving a number of problems for low-mass satellites, here we use the Starkenburg et al. (2013) model to focus on the faint galaxies in the field. Although the Aquarius simulation high-resolution box is small (∼2.4 h^{-1}Mpc on a side), it is large enough to contain several hundred small galaxies whose properties can be contrasted to observations. By focusing on systems in the field, and specifically on central galaxies, we should also be able to establish if the gas content of our galaxies is modelled properly and whether the mismatch found for the satellites is only due to environmental effects.

This paper is organized as follows. We describe the most relevant characteristics of our SA method in Section 2. In Section 3, we compare the LF, H I mass function and the velocity function for the galaxies in the SA model to those in the ALFALFA sample from Papastergis et al. (2015). We explore in this section the reasons behind the success of this comparison, and on the failure of abundance matching methods on the lower mass end. In Section 4, we summarize our results and conclusions.

2 METHODOLOGY

Starkenburg et al. (2013) have used the Aquarius dark matter simulations in combination with an SA galaxy formation model that stems originally from De Lucia, Kauffmann & White (2004), Croton et al. (2006), De Lucia & Blaizot (2007); De Lucia & Helmi (2008) and Li et al. (2010). The Aquarius haloes were identified in the Millennium-II Simulation (Boylan-Kolchin et al. 2009), a cosmological N-body simulation with the following parameters: $\Omega_{\rm m} = 0.25$, $\Omega_\Lambda = 0.75$, $\sigma_8 = 0.9$, $n_{\rm s} = 1$, $h = 0.73$ and $H_0 = 100\,h$ km s^{-1} Mpc. A series of five zoom-in simulations with progressively higher resolution centred around six different MW mass haloes were performed, until a particle mass resolution of $m_{\rm p} \sim 1.7 \times 10^3$ M$_\odot$ and spatial resolution of ∼20 pc were achieved (Springel et al. 2008). The SA model of Starkenburg et al. (2013) follows a number of important physical processes that affect the evolution of a galaxy, including star formation, feedback, cooling, heating, mergers, etc. We briefly describe here in more depth those processes that have an important effect on low-mass galaxies, and refer the reader to the papers mentioned earlier for more details. In summary:

(i) The feedback model corresponds to the De Lucia et al. (2004) prescription, in which the gas mass that is reheated by supernovae feedback is $\propto E_{\rm SN}/V_{\rm vir}^2 \Delta M_*$, i.e. it is inversely proportional to the depth of the potential-well (as given by its virial velocity $V_{\rm vir}$) and proportional to the amount of newly formed stars ΔM_*.

(ii) Reionization is modelled following the simulations of Gnedin (2000), who quantified the effect of photoionization/photoevaporation on low-mass haloes. This effectively leads to a reduction in the baryon content in haloes below a 'filtering mass', given by

$$f_{\rm b,halo}(z, M_{\rm vir}) = f_{\rm b}[1 + 0.26 M_{\rm F}(z)/M_{\rm vir}]^3, \quad (1)$$

where $f_{\rm b} = 0.17$ is the universal baryon fraction. For $M_{\rm F}(z)$, the analytical fitting function from appendix B in Kravtsov, Gnedin & Klypin (2004) is used.[1] Reionization is assumed to start at redshift $z_0 = 15$ and end at $z_{\rm r} = 11.5$. Although this may be on the high-redshift end of plausible values (Planck Collaboration I 2014), it is important to realize that the Aquarius simulations represent an overdense environment in which reionization may well have started earlier.

(iii) Cooling depends on metallicity and temperature of the hot gas. Cooling via molecular hydrogen is assumed to be highly inefficient and prevented by photodissociation caused by UV radiation from the stars, especially at early times (Haiman et al. 2000), and

[1] The second line in equation (B2) of this paper contains a type-setting error, which has been fixed in the version on the arXiv.

in the model it is forbidden for haloes below the atomic hydrogen cooling limit, $T_{\rm vir} = 10^4$ K, where

$$T_{\rm vir} = 35.9(V_{\rm vir}/{\rm km\,s^{-1}})^2. \quad (2)$$

(iv) Star Formation in the quiescent mode (as opposed to in starbursts) is assumed to take place in an exponential thin disc of radial scalelength $r_{\rm d}$. The mass in cold gas of the disc that is in excess of critical threshold $M_{\rm crit}$ is transformed into stars:

$$M_{\rm crit} = 1.14 \times 10^8 (V_{\rm vir}/20\ {\rm km\,s^{-1}})(r_{\rm d}/1\ {\rm kpc}){\rm M}_\odot, \quad (3)$$

where this criterion effectively stems from the surface density critical threshold for star formation found by Kennicutt (1998). The value of $r_{\rm d}$ is calculated as in De Lucia & Helmi (2008), assuming conservation of specific angular momentum of the gas as it cools and settles into a rotationally supported disc (following Mo, Mao & White 1998). However, it is recomputed at each time-step by taking the mass-weighted average profile of the gas disc already present and that of the new material being accreted.

The luminosities of our galaxies are computed from the stellar masses using stellar population synthesis models from Bruzual & Charlot (2003), and assuming a Chabrier initial mass function (Chabrier 2003), as in De Lucia & Blaizot (2007).

In what follows, we use the Aquarius series of haloes resolution level-2 (hereafter, Aq-A-2, Aq-B-2, Aq-C-2, Aq-D-2, Aq-E-2 and Aq-F-2) coupled to our SA model to analyse different galaxy properties and compare them with observations. To assess the numerical convergence of the model, we use four resolution levels of the Aq-A halo. Each of these simulations encompass a high-resolution region of radius $\sim$1.2 Mpc h^{-1} that extends well outside the virial radius of the main MW-like haloes. The 'field (or central) haloes' (i.e. not satellites) located in this region are largely the focus of the current study.

The upper panel of Fig. 1 shows the virial mass function of central haloes within 1.2 Mpc h^{-1} from the MW-like galaxies for the different Aquarius level-2 haloes (coloured lines). The lower panel shows the good convergence of the virial mass function of the Aq-A halo in the four different resolutions. The vertical lines show the different $M_{\rm vir}$ thresholds above which the mass function has converged for each resolution level. The error bars in these plots, as well as similar figures in the rest of the paper, correspond to 1σ uncertainties assuming Poisson errors on the counts of each individual bin. In both panels, the grey dotted line corresponds to the Reed et al. (2007) mass function fit (using the Press–Schechter option in the code provided by these authors).

The LF, i.e. the abundance of galaxies with a given luminosity, is shown in Fig. 2 for our model. The top panel shows the LFs including central and satellite galaxies, while the bottom two are only for centrals. Different colours correspond to galaxies residing in the different Aquarius level-2 simulations.

To normalize these curves, and take into account the relatively small volume sampled by the Aquarius simulations, we computed $N_{\rm Mill}$, the mean number density of galaxies with B-band absolute magnitude in the range $-18 < M_{\rm B} < -14$ in the milli-Millenium catalogue[2] which uses the SA model of De Lucia & Blaizot (2007). In the same way, we computed $N_{\rm AQ}$ for each of the Aquarius simulations, and estimated the normalization factor as $\log f = \log N_{\rm AQ}/N_{\rm Mill}$. Using only central galaxies, this is found to vary from 0.55 for Aq-E to 0.85 for Aq-A, and this variation

[2] http://gavo.mpa-garching.mpg.de/Millennium/

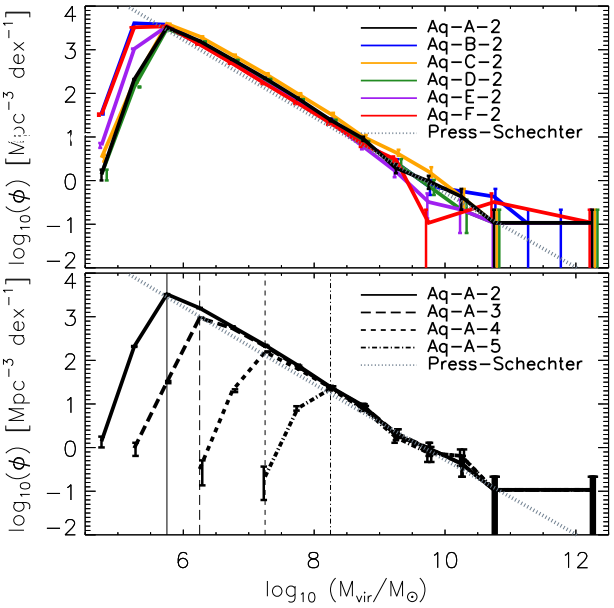

Figure 1. Upper panel: virial mass function of central haloes within 1.2 Mpc h^{-1} from the MW for all six Aquarius level-2 simulations (coloured lines). The dotted grey line corresponds to the fit to the mass function in our simulations using the publicly available code from Reed et al. (2007). Lower panel: virial mass function of the Aq-A halo for four different resolutions for central haloes within 1.2 Mpc h^{-1} from the MW (black lines). The vertical lines show the different $M_{\rm vir}$ threshold, according to each resolution: Aq-A-2 = $10^{5.5}$ M$_\odot$, Aq-A-3 = 10^6 M$_\odot$, Aq-A-4 = 10^7 M$_\odot$, Aq-A-5 = 10^8 M$_\odot$.

is simply due to small number statistics. Therefore, we have decide to take an average normalization factor $\log f = 0.7$ and applied this normalization to all our simulations. When using central and satellite galaxies still embedded in their own subhalo, the average normalization factor is, as expected, only slightly different, with $\log f = 0.8$. Depending on the systems shown, these normalizations are also applied in Figs 3 and 5. The black lines in the bottom panel of Fig. 2 show how well the LF has converged by comparing the results for the four different resolutions for central galaxies in the Aq-A series.

Many studies have estimated the LF in the field (e.g. Norberg et al. 2002; Bell et al. 2003; Blanton et al. 2005; Trujillo-Gomez et al. 2011); however, for the current study, it is important to know its shape at the faint end. This is why we compare here to the LF derived by Klypin et al. (2015). These authors have used the current version of Updated Nearby Catalogue (Karachentsev, Makarov & Kaisina 2013) which contains 869 galaxies with redshift-independent distances $D < 11$ Mpc or radial velocities with respect to centroid of the Local Group $V_{\rm LG} < 600$ km s^{-1}. We focus on the subsample with distances $D \leq 10$ Mpc, which comprises 733 galaxies, of which 652 objects are brighter than B-band absolute magnitude $M_{\rm B} = -10$ and 426 are brighter than $M_{\rm B} = -13$. The grey filled circles in Fig. 2 represent the resulting LF, while the dotted grey curve presents a Schechter fit to this sample for galaxies with $M_{\rm B} < -14$, with the following Schechter parameters: $\phi^* = 1.25 \times 10^{-2}\,h^3$ Mpc^{-3}, $\alpha = 1.3$ and $M_{*,{\rm B}} = -20.0 + 5\log(h)$ (equation 2 of Klypin et al. 2015).

This comparison shows that there is reasonable agreement between our model and the field LF for $M_{\rm B} < -14$. The inclusion of satellites in the models does not lead to a drastic change in the shape or normalization of the LF, especially if we consider the

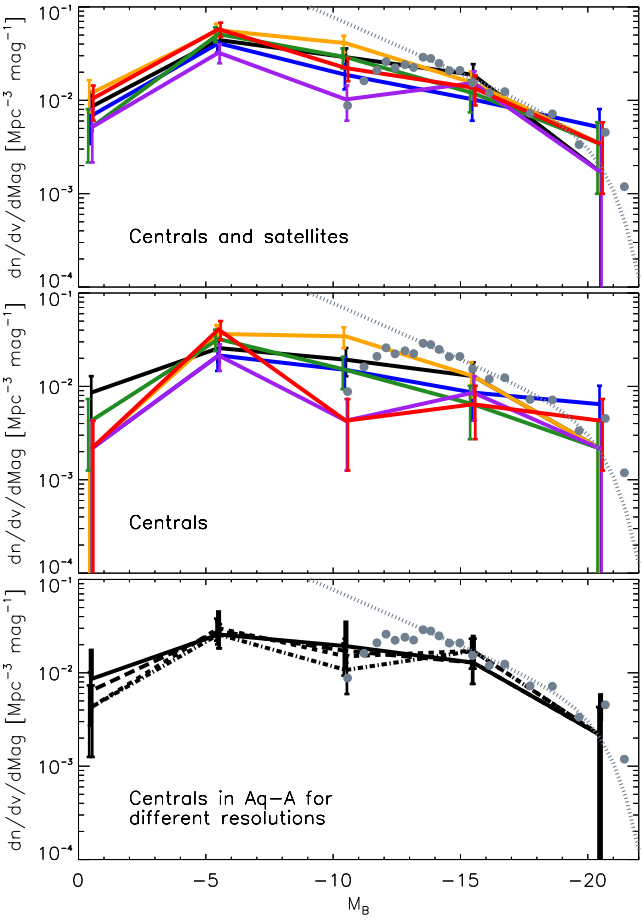

Figure 2. Upper panel: luminosity function of central and satellites galaxies with $M_{vir} > 10^{5.5}$ $M_\odot$ and within 1.2 Mpc h^{-1} from the main MW-like galaxy for all six haloes in the Aquarius level-2 series (colours follow same scheme as in Fig. 1). The grey filled circles are from Klypin et al. (2015) while the dotted grey curve shows the Schechter fit: $\phi^* = 1.25 \times 10^{-2}$ Mpc^{-3}, $\alpha = 1.3$ and $M_{*,B} = -20.0 + 5\log(h)$. Middle and bottom panels: luminosity function for central galaxies only. In the bottom panel, only those of the Aq-A halo are shown for four different resolutions, and evidence the good convergence of the models.

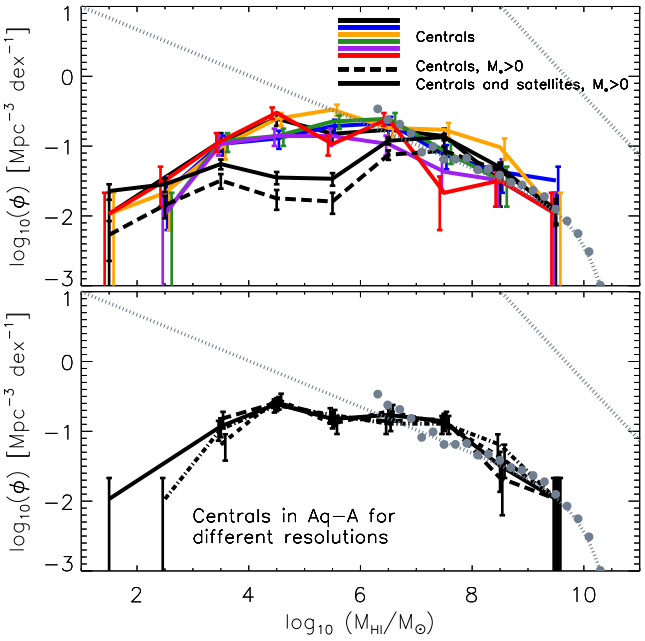

Figure 3. Upper panel: H I mass function of central galaxies for all six haloes of Aq-2, with $M_{vir} > 10^{5.5}$ $M_\odot$ and within 1.2 Mpc h^{-1} from the MW (colour solid lines). The dashed curve shows the H I mass function for central galaxies containing both stars and gas, while the dot–dashed curve includes also satellite galaxies. Grey filled circles represent the H I mass function estimated while the grey dotted line is the Schechter function fit: $\phi^* = 0.0048$, $\log(M_*) = 9.96$ and $\alpha = -1.33$ (Martin et al. 2010). The grey dotted line at the upper right-hand corner is the halo mass function. Lower panel: H I mass function of the Aq-A halo for four different resolutions for central galaxies within 1.2 Mpc h^{-1} from the MW (black lines). We use different M_{vir} thresholds for each resolution.

important scatter from simulation to simulation. This is a consequence of the small volume (and hence relatively small number of objects) of the high-resolution region of the Aquarius haloes. Coupled to possible incompleteness in the data for galaxies with $M_B > -12$, and the somewhat arbitrary normalization, it is hard to argue that the modelling needs any improvement.

3 RESULTS ON THE H I MASS FUNCTION AND VELOCITY FUNCTION

3.1 Neutral hydrogen (H I) mass function

Figs 1 and 2 confirm that the virial mass function of haloes and the LF of galaxies have very different slopes at the low-mass end. To further explore this difference, we now focus on the H I mass function. This offers an independent test of the model because in low-mass systems, the baryonic budget is dominated by gas rather than by stars.

In the upper panel of Fig. 3, we show the H I mass functions of central galaxies for all six Aquarius level–2 haloes, for which $M_{vir} > 10^{5.5}$ $M_\odot$ and located, as before, in the high-resolution box around the main MW-like galaxies. Each colour corresponds to a different halo. The black dashed line shows the H I mass function for central systems that have both cold gas and stars, and is the average over all Aquarius level–2 haloes. It evidences that many objects with cold gas (with $M_{HI} < 10^6 M_\odot$) have not been able to form any stars (see discussion below). The dot–dashed curve represents the corresponding H I mass function but now including both central and satellite galaxies, i.e. these are the counterparts of the objects shown in the top panel of Fig. 2. Note that the two curves follow each other relatively well, and are only offset by ∼0.2 dex at $M_{HI} \sim 10^{7.5} M_\odot$. This difference, due to satellite galaxies baring H I, is relatively small in comparison to the scatter from simulation to simulation. The black lines in the bottom panel of this figure show the H I mass function of the Aq-A halo for the four different resolutions and again indicate very good convergence.

Martin et al. (2010) have derived the H I mass function from a sample of ∼10^4 extragalactic sources comprising the ALFALFA 40 per cent survey (hereafter α.40), with $6.2 < \log(M_{HI}/M_\odot) < 11.0$. These are plotted as the grey filled circles in Fig. 3. The grey dotted line is the Schechter function fit to this data set with the parameters: $\phi^* = 0.0048$, $\log(M_*) = 9.96$ and $\alpha = -1.33$ as estimated by Martin et al. (2010).

The top panel of Fig. 3 shows that there is good agreement between the observed H I mass function of galaxies with $M_{HI} \sim 10^{6.5} - 10^9 M_\odot$ and our models. There are, in fact, three comparisons to be made: (i) with all central galaxies (including those

without a stellar component, the coloured curves); (ii) with central systems that host a luminous galaxy (dashed black curve); and (iii) with centrals and satellites hosting a luminous galaxy (dot–dashed curve). One of the reasons to consider these three classes separately rests on our aim to establish if the H I contents of central galaxies (in the field) are consistent with observations, in particular in relation to gauging the impact of environmental effects such as ram pressure stripping on satellites. Note that in all cases, at the high-mass end, our simulation box is too small and does not contain enough galaxies, as evidenced by the large error bars in this figure.

The first point to note is the relatively large scatter from simulation to simulation at intermediate masses for central galaxies, although all curves are consistent within 1σ of each other, and on average also consistent with the observed H I mass function. However, since most objects observed in the ALFALFA survey actually have an optical counterpart (see e.g. Haynes et al. 2011), a better comparison to make is to the dashed black curve, representing central luminous galaxies. We note the excellent agreement with the observations at these masses, although for masses $M < 10^6\,\mathrm{M}_\odot$, the predicted H I mass function appears to decline to a point that may be in tension with the observations. On the other hand, it is possible that satellite galaxies are present in the observational sample. As expected, when these are included in the predicted H I mass function, there is an increase in the number of objects although the agreement with the observations is still very reasonable. This implies that ram pressure stripping, although it should be included when modelling the properties of satellite galaxies, will not result in dramatic changes that will break-down the good agreement between the models and the observations, at least for the range of masses probed by the latter.

More careful comparisons, especially regarding the low-mass end of the H I mass function and the presence of systems without a stellar counterpart, are necessary. It will be important to have both deeper surveys in H I as well as in the optical, as these will allow us to establish whether the trends predicted are correct.

In the top panel of Fig. 4, we have plotted the *B*-band absolute magnitude against the virial mass for all the 173 central galaxies in the high-resolution region of the Aquarius haloes. The panel below shows the H I mass against the virial mass for all these galaxies as red circles, while the open circles denote objects that according to our SA model have not formed any stars ($M_* = 0$) but do contain cold gas. There are 315 such objects with $M_{\rm vir} \geq 10^{5.5}\mathrm{M}_\odot$. The reason such systems do not form stars is because their surface gas density is below the threshold for star formation imposed by our model.

An estimate of the dependence of the critical mass on the virial mass of objects can be obtained using equation (3). In that equation, we replace the disc radial scalelength by $\tilde{r}_{\rm d} = \lambda r_{\rm vir}/\sqrt{2}$, where λ is the dimensionless spin parameter (which we take to be $\sim$0.035) and $r_{\rm vir}$ the virial radius of the host halo. As explained earlier, this scale is obtained assuming conservation of specific angular momentum, and that when hot gas cools at the centre of dark matter haloes, it settles in a rotationally supported disc (Mo et al. 1998). The value of $\tilde{r}_{\rm d}$ will typically be larger than $r_{\rm d}$, because the latter is a mass-weighted average over the whole gas cooling history of the system. Therefore $\tilde{M}_{\rm crit}$ obtained in this way will be overestimated in general. Nonetheless, this rough zero order approximation of the critical mass is plotted as the line in the bottom panel. This comparison serves to tentatively support our claim that the density of cold gas in lower mass objects is too low to allow star formation taking place.

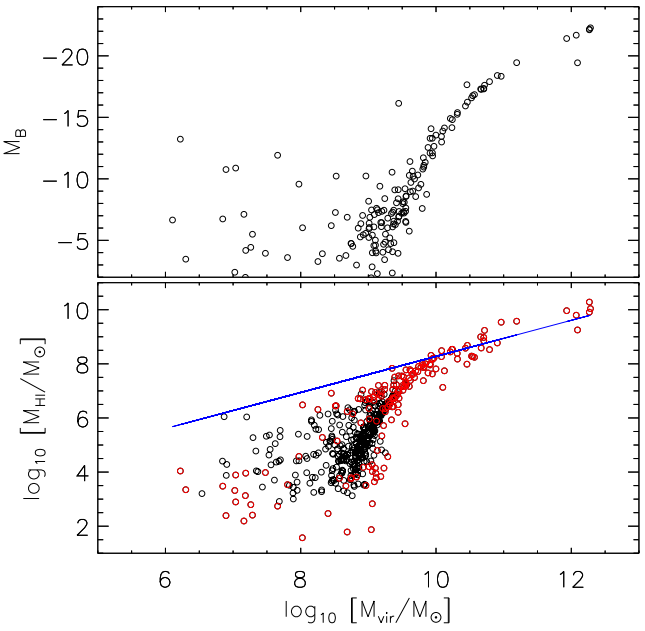

Figure 4. Upper panel: $M_{\rm B}$ versus $M_{\rm vir}$ for all the central galaxies in our models. Lower panel: $M_{\rm H\,I}$ versus $M_{\rm vir}$ for objects with stars (red circles) and for those with only gas (black circles). The line shows $\tilde{M}_{\rm crit}$, an upper limit estimate of the critical mass above which a halo would form stars.

It should also be borne in mind that since the criterion given by equation (3) for the critical mass of gas for star formation is strict and global, it is likely that if some stochasticity would be allowed and density variations inside a system considered, that some systems below the threshold should be able to form stars. This implies that the exact predictions for the shape of the H I mass function for objects around and below $M_{\rm crit}$ should be taken with a grain of salt.

This analysis supports the idea that ram pressure stripping of gas once a system becomes a satellite will not affect the properties of the objects significantly. Most of the gas present in the systems has too low density to form stars, which is also why the LF of galaxies (including satellites) is in agreement with observations, even if in our model, ram pressure has not really been implemented. For this reason, in the remainder of this paper we only focus on the behaviour of central galaxies.

3.2 Velocity function

So far we have compared the observed global baryonic properties of galaxies to those in our models. An additional important complementary aspect concerns the internal dynamics of galaxies, which links the galaxies to their host dark matter haloes. A fundamental question that potentially relates to the nature of dark matter, is whether the galaxies in the SA model are hosted by the right dark matter haloes in the simulations.

This is why we now focus on velocity function, namely the abundance of galaxies with a given circular velocity (Cole & Kaiser 1989; Shimasaku 1993; Gonzalez et al. 2000; Zavala et al. 2009; Trujillo-Gomez et al. 2011). To measure circular velocities for large numbers of galaxies is challenging, but wide-area, single-dish 21 cm surveys are making this possible. Although ideally one would like to obtain full rotation curves for a large number of systems spanning a large range in galaxy mass, this is too time consuming to be currently feasible. Therefore, what is rather used is the width of the spectral H I line profile w. This is believed to be close to the

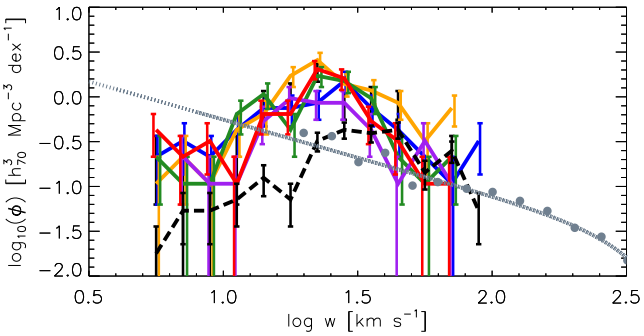

Figure 5. Velocity width function of central galaxies within 1.2 Mpc h^{-1} from the centre of the MW-like Aquarius haloes, with $M_{\rm HI} > 10^4$ M$_\odot$ and with M$_{\rm vir} > 10^{5.5}$ M$_\odot$ for the all six haloes of resolution level-2 (coloured lines). The dashed curve is the average over all size Aquarius haloes taking into account only those systems hosting also stars. Grey filled circles represent the measured ALFALFA WF, and dotted grey curve represents the fit of the modified Schechter function: $\phi^* = 0.011\,h^3_{70}$ Mpc^{-3}, log $w_* = 2.58$, $\alpha = -0.85$ and $\beta = 2.7$ (Papastergis et al. 2011).

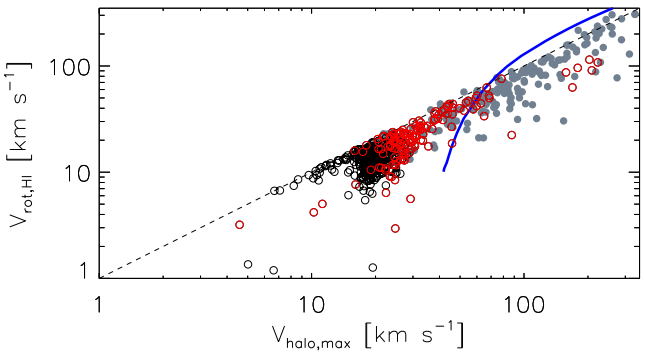

Figure 6. Distribution of $v_{\rm rot}$ versus $V_{\rm max}$ for the data set from Papastergis et al. (2015) (grey solid points), for the dark matter haloes hosting our model galaxies (red circles), and for systems in our model that have $M_* = 0$ but $M_{\rm HI} > 10^4$M$_\odot$ (black circles). The blue curve shows the relation predicted by abundance matching given by Papastergis et al. (2015). The luminous central galaxies in our model occupy the same region as the observations. Note that for $V_{\rm max} > 100$ km s^{-1}, the rotational velocities of the observed galaxies are systematically higher. This merely reflects that the baryon contribution (which is not taken into account for the model galaxies), is non-negligible for these systems.

peak rotational velocity of the system at approximately two radial scalelengths.

Papastergis et al. (2011) have measured the velocity width function (WF) of H I-bearing galaxies down to $w = 20$ km s^{-1} in the ALFALFA survey. This WF is based on 10 744 H I-selected galaxies from the $\alpha.40$ survey (a more than twofold increase over previous data sets), so it is the largest H I-selected sample to date.

For each dark matter halo in the Aquarius suite, Springel et al. (2008) has derived the peak circular velocity $V_{\rm max}$ and the circular velocity at the virial radius $v_{\rm c}(r_{\rm vir}) = V_{\rm vir}$, as well as the location of the peak $r_{\rm max}$ and the virial radius $r_{\rm vir}$. With this information, and assuming an Navarro-Frenk-White (NFW) shape, we may derive the full form of the rotation curve. Furthermore, we may derive $v_{\rm rot}$, i.e. $v_{\rm c}(2r_{\rm d})$ using the value of $r_{\rm d}$ as determined from our SA model.[3]

To compare this data with the results of Papastergis et al. (2011), we convert rotational velocities into H I velocity widths by assuming the relationship given by equation (4) of Papastergis et al. (2011):

$$w = 2v_{\rm rot} \sin i + w_{\rm eff}. \quad (4)$$

This equation indicates that the galaxies are randomly oriented with respect to the line of sight ($\cos i$ is uniformly distributed in the [0, 1] interval), while $w_{\rm eff}$ is a small 'effective' term used to reproduce the broadening effect of turbulence and non-circular motions on H I linewidths. Following Papastergis et al. (2011), we consider $w_{\rm eff} = 5$ km s^{-1} for the broadening term, which is added linearly for galaxies with $v_{\rm rot} > 50$ km s^{-1} and in quadrature for lower velocity galaxies.

Fig. 5 shows the resulting velocity WF of the same central galaxies as in previous plots, with $M_{\rm HI} > 10^4$ M$_\odot$ and with $M_{\rm vir} > 10^{5.5}$ M$_\odot$ for the all six haloes of resolution level-2 in the Aquarius suite (coloured lines). The velocity function considering only systems with a stellar counterpart (i.e. $M_* > 0$) averaged over all six Aquarius haloes is shown as the dashed black curve.

The grey filled circles in the same figure represent the measured ALFALFA WF presented by Papastergis et al. (2011), based on galaxies which are positioned in the portion of the flux-width plane where the ALFALFA survey is complete and have profile widths broader than $w \gtrsim 20$ km s^{-1}. The dotted grey curve represents the fit of the modified Schechter function (equation 2 of Papastergis et al. 2011) with the following parameters: $\phi_* = 0.011h^3_{70}$ Mpc^{-3} dex^{-1}, log $w_* = 2.58$, $\alpha = -0.85$, and $\beta = 2.7$ (Papastergis et al. 2011).

The agreement between the predictions of the model and the observations is quite good. It shows that our model places galaxies of the right baryonic content (in stars and in H I gas) in the 'right' dark matter haloes. Contrary to previous work (see e.g. Papastergis et al. 2015, and references therein), our model does not present an excess of luminous galaxies with too low velocity widths compared to the observations. The resulting function has a similar slope as observed.

It is interesting to note that in our model, those systems with cold gas but lacking stars, lead to an excess above the Schechter function that fits so well the luminous galaxies in our model. This excess only appears for log $w \sim 1.2 - 1.5$, which is right around, and slightly below the limit of the ALFALFA survey.

3.3 Zooming into the properties of galaxies and their host haloes

Our models do not appear to have a significant excess of haloes hosting galaxies of a given velocity width w at the faint-/low-mass end. To understand furthermore this result, we now zoom into the properties of the haloes hosting galaxies.

Papastergis et al. (2015) analysed the kinematics of a sample of gas-rich dwarf galaxies extracted from the literature. They derived $v_{\rm rot}$ by making inclination corrections using Sloan Digital Sky Survey (SDSS) images, and estimated the value of $V_{\rm max}$ by considering the most massive halo that is consistent with the last measured point of the rotation curves available for these galaxies.

In Fig. 6, we show the distribution of $v_{\rm rot}$ versus $V_{\rm max}$ for this data set (grey solid points) as well as for the central dark matter haloes hosting our model galaxies (red circles). With black open circles with indicate those systems in our model that have $M_* = 0$ but $M_{\rm HI} > 10^4$M$_\odot$, i.e. they are devoid of stars, and hence would not be in the observational compilation of Papastergis et al. (2015).

[3] Our results do not change significantly if we instead compute the circular velocity at $r_{\rm d}$ or at $3r_{\rm d}$.

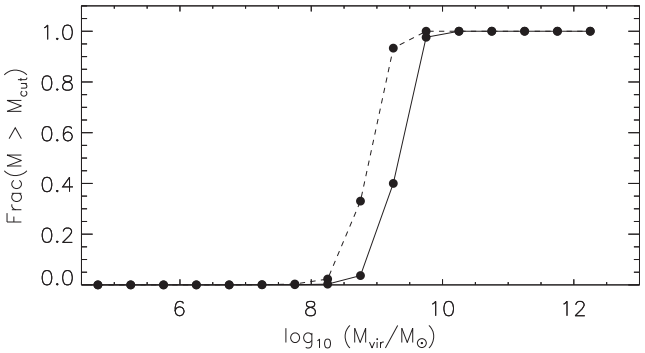

Figure 7. Fraction of haloes hosting a luminous galaxy with $M_* > 10^3 M_\odot$ (solid) and haloes with more than $10^4 M_\odot$ H I gas (dashed) as function of $M_{\rm vir}$.

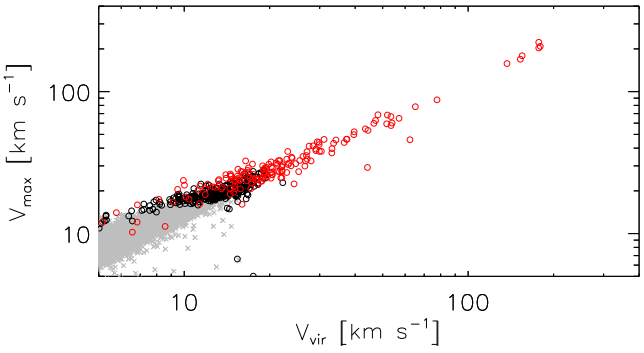

Figure 8. Distribution of $V_{\rm vir}$ versus $V_{\rm max}$ for the central dark matter haloes hosting our model galaxies (red circles), for systems in our model that have $M_* = 0$ but $M_{\rm HI} > 10^4 M_\odot$ (black open circles) and for completely dark haloes (grey crosses).

The blue curve shows the relation predicted by abundance matching according to Papastergis et al. (2015).

This comparison is extremely satisfactory and confirms again that model galaxies are placed in the right host dark matter haloes. No discrepancies are found, and there is no evidence from this plot that the dark matter haloes in the simulations would be too massive or too dense to host the observed galaxies.

However, this is in tension with the naive conclusion that one would have drawn from comparing the observations to the predictions of abundance matching. It is important therefore to understand why the galaxies in our model do not follow the predictions of abundance matching. Equally important it is to understand why only haloes with $V_{\rm max} > 20\,{\rm km\,s^{-1}}$ host luminous galaxies.

The reason that abundance matching does not work at the low-mass end of the halo spectrum is that the ability of a halo to host a galaxy depends on its capacity to (i) retain the baryons; (ii) cool gas from the hot phase; and (iii) have enough cold gas at high density for star formation. These conditions are redshift dependent, and hence the virial mass or velocity at the present-day are not sufficient to establish whether a halo will host a galaxy (unless this mass is significantly different from the various thresholds). Of the haloes that are near the thresholds for these physical processes to take place, some fraction will satisfy these requirement, and this fraction is not fully random, and is not mass ranked (as in abundance matching) but depends on the specific history of the halo.

This point is made clear by considering the fraction of central haloes that host galaxies as a function of virial mass. This is plotted in Fig. 7, where the fraction of galaxies with $M_* > 10^3 M_\odot$ at a given $M_{\rm vir}$ is indicated by the solid line, and the fraction of systems with $M_{\rm HI} > 10^4 M_\odot$ is given by the dashed line. From this figure, we see that all haloes with $M_{\rm vir} > 10^{10} M_\odot$ host luminous galaxies, while only 50 per cent of those with $M_{\rm vir} \sim 10^{9.4} M_\odot$ do. On the other hand, this function is shifted to lower masses if we consider the systems with cold gas: 50 per cent of the haloes with $M_{\rm vir} = 10^{8.9} M_\odot$ contain H I. This shift is present because, not only must a halo be able to cool gas but in order to form stars, this gas must be above the threshold for star formation. It is also interesting that these functions are not exactly steps, and this is a manifestation of the various processes at work which have different thresholds, as discussed above.

Fig. 8 shows the $V_{\rm max}$ versus $V_{\rm vir}$ for the central model galaxies as red circles, the systems with no stars but with $M_{\rm HI} > 10^4 M_\odot$ as open black circles, and the dark matter haloes without baryons as grey crosses. This demonstrates clearly that virial velocity today $V_{\rm vir}$ is not enough to predict if a halo will host a luminous galaxy. It also shows that at a given $V_{\rm vir}$, luminous galaxies are hosted in haloes with higher $V_{\rm max}$. This implies that for a given $V_{\rm vir}$, these are the most concentrated haloes since for a NFW halo:

$$V_{\rm max} = 0.465 V_{\rm vir} \left(\frac{c}{f(c)} \right)^{1/2} \quad (5)$$

and

$$f(c) = \ln(1+c) - c/(1+c), \quad (6)$$

where $c = r_{\rm vir}/r_{\rm s}$ is the concentration, with $r_{\rm s}$ the scale radius of the halo. These more concentrated haloes will have typically collapsed earlier, implying that they reach a higher mass at earlier times which therefore increases their likelihood of being above e.g. the H I cooling limit at which point they can start forming stars if they have retained enough baryons (after photoevaporation).

This also explains why the hosts of luminous galaxies are to the left of the abundance matching curves, since

$$\frac{V_{\rm rot}^2}{V_{\rm max}^2} = 4.63 \frac{f(x)}{x}, \quad (7)$$

where $f(x)$ is given by equation (6) with $x = 2r_{\rm d}/r_{\rm s}$. In general, we can assume that $x \lesssim 2$ (i.e. $r_{\rm d} < r_{\rm s}$), in which case $f(x)/x$, increases with increasing x. This implies that for fixed $r_{\rm d}$, galaxies with smaller $r_{\rm s}$ (i.e. in more concentrated haloes), have larger $V_{\rm rot}/V_{\rm max}$. In other words, $V_{\rm max}$ at fixed $V_{\rm rot}$ is lower for more concentrated haloes. This highlights that for abundance matching to work, it is important to select haloes that are most concentrated amongst those that are near the thresholds.

Fig. 8 shows that dark haloes (grey crosses) have $V_{\rm vir} < 20\,{\rm km\,s^{-1}}$, which is consistent with the fact that the H I cooling limit is $V_{\rm vir}^{\rm cool} \sim 16.7\,{\rm km\,s^{-1}}$. Equation (5) explains why basically all objects with $V_{\rm max} \lesssim 20\,{\rm km\,s^{-1}}$ are dark, as the function $\sqrt{c/f(c)}$ is weakly dependent on c. Since haloes hosting luminous galaxies are on average in more concentrated haloes as discussed above, their $V_{\rm max}$ is higher as seen in this figure.

4 CONCLUSIONS

We have used the high-resolution Aquarius cosmological dark matter simulations in combination with the SA model by Starkenburg et al. (2013) to study the H I content and dynamical properties of galaxies at the low-mass end in the context of the ΛCDM paradigm. We have compared our predictions to the observed ALFALFA survey, and found excellent agreement with the H I mass and velocity WFs measured by this survey for central galaxies, down to the lowest

mass scales probed. Implicit in this conclusion, is our assumption that luminous satellite galaxies do not contribute significantly to these H I distribution functions. This is based on the fact that even if these systems are considered when computing the model H I mass function, we still find good agreement with observations, and the same is true for the LF. Therefore, even if we do not include the effect of ram pressure stripping in our models explicitly, we argue that its effect will not lead to dramatic changes in the properties of galaxies. This is because the gas that is present in these systems is too diffuse to contribute to star formation, and hence have an impact on the evolution of these objects.

We have also studied the relation between two global parameters of the circular velocity curves of the galaxies in our models and in the ALFALFA survey, namely between their peak velocity and circular velocity at two radial disc scalelengths. The distribution found in our models overlaps perfectly with that inferred from observations. This suggests that our galaxies are placed in the right dark matter haloes, and consequently and at face value we do not seem to find any discrepancy with the predictions from the ΛCDM model.

Our model predicts the existence of a population of H I haloes that do not have a stellar counterpart (e.g. Salvadori & Ferrara 2012). The exact abundance of these objects is likely to depend rather strongly on the implementation of star formation in the models, including whether cooling below 10^4 K is allowed (via H_2) and on the critical density floor for star formation. Although these objects are relatively gas-rich, their cold gas is too diffuse. Furthermore, their baryon fraction is well below universal, since typically $f_b \leq 0.01$, reflecting the fact that they lost an important fraction of baryons because of photoevaporation during reionization.

ACKNOWLEDGEMENTS

We are grateful to Manolis Papastergis and Simon White for interesting discussions and the Aquarius project members, especially to Volker Springel. We are also indebted to Gabriella De Lucia and Yang-Shyang Li for the numerous contributions in the development of the SA code used here. The referee, Darren Croton, is acknowledged for a very positive and constructive report that has helped improve the manuscript. This work has been partially supported by the Consejo de Investigaciones Científicas y Técnicas de la República Argentina (CONICET), by the Secretaría de Ciencia y Técnica de la Universidad Nacional de Córdoba (SeCyT) and by the European Commissions Framework Programme 7, through the International Research Staff Ex–change Scheme LACEGAL. AH acknowledges financial support from the European Research Council under ERC–StG grant GALACTICA–240271. AH and MA acknowledge grant PICT1137 from FONCYT Argentina. ES acknowledges partial funding from the Canadian Istitute for Advanced Research (CIFAR).

REFERENCES

Barkana R., Loeb A., 1999, ApJ, 523, 54
Bell E. F., McIntosh D. H., Katz N., Weinberg M. D., 2003, ApJS, 149, 289
Blanton M. R., Eisenstein D., Hogg D. W., Schlegel D. J., Brinkmann J., 2005, ApJ, 629, 143
Bode P., Ostriker J. P., Turok N., 2001, ApJ, 556, 93
Boylan-Kolchin M., Springel V., White S. D. M., Jenkins A., Lemson G., 2009, MNRAS, 398, 1150
Boylan-Kolchin M., Bullock J. S., Kaplinghat M., 2012, MNRAS, 422, 1203
Bruzual G., Charlot S., 2003, MNRAS, 344, 1000
Bullock J. S., Kravtsov A. V., Weinberg D. H., 2001, ApJ, 548, 33
Chabrier G., 2003, PASP, 115, 763
Cole S., Kaiser N., 1989, MNRAS, 237, 1127
Colín P., Avila-Reese V., Valenzuela O., 2000, ApJ, 542, 622
Croton D. J. et al., 2006, MNRAS, 365, 11
De Lucia G., Blaizot J., 2007, MNRAS, 375, 2
De Lucia G., Helmi A., 2008, MNRAS, 391, 14
De Lucia G., Kauffmann G., White S. D. M., 2004, MNRAS, 349, 1101
Dekel A., Silk J., 1986, ApJ, 303, 39
Ferrero I., Abadi M. G., Navarro J. F., Sales L. V., Gurovich S., 2012, MNRAS, 425, 2817
Garrison-Kimmel S., Boylan-Kolchin M., Bullock J. S., Lee K., 2014, MNRAS, 438, 2578
Gnedin N. Y., 2000, ApJ, 542, 535
Gonzalez A. H., Williams K. A., Bullock J. S., Kolatt T. S., Primack J. R., 2000, ApJ, 528, 145
Governato F. et al., 2012, MNRAS, 422, 1231
Haiman Z., Abel T., Rees M. J., 2000, ApJ, 534, 11
Haynes M. P. et al., 2011, AJ, 142, 170
Kamionkowski M., Liddle A. R., 2000, Phys. Rev. Lett., 84, 4525
Karachentsev I. D., Makarov D. I., Kaisina E. I., 2013, AJ, 145, 101
Kennedy R., Frenk C., Cole S., Benson A., 2014, MNRAS, 442, 2487
Kennicutt R. C., Jr, 1998, ApJ, 498, 541
Klypin A., Kravtsov A. V., Valenzuela O., Prada F., 1999, ApJ, 522, 82
Klypin A., Karachentsev I., Makarov D., Nasonova O., 2015, MNRAS, 454, 1798
Komatsu E., Smith K. M., Dunkley J., Bennett C. L., 2011, ApJS, 192, 18
Kravtsov A., 2010, Adv. Astron., 2010, 8
Kravtsov A. V., Gnedin O. Y., Klypin A. A., 2004, ApJ, 609, 482
Li Y.-S., De Lucia G., Helmi A., 2010, MNRAS, 401, 2036
Mac Low M. M., Ferrara A., 1999, ApJ, 513, 142
Martin A. M., Papastergis E., Giovanelli R., Haynes M. P., Springob C. M., Stierwalt S., 2010, ApJ, 723, 1359
Mo H. J., Mao S., White S. D. M., 1998, MNRAS, 295, 319
Moore B., Ghigna S., Governato F., Lake G., Quinn T., Stadel J., Tozzi P., 1999, ApJ, 524, L19
Norberg P., Cole S., Baugh C. M., Frenk C. S., Baldry I., Bland-Hawthorn J., Bridges T., 2002, MNRAS, 336, 907
Obreschkow D., Ma X., Meyer M., Power C., Zwaan M., Staveley-Smith L., Drinkwater M. J., 2013, ApJ, 766, 137
Papastergis E., Martin A. M., Giovanelli R., Haynes M. P., 2011, ApJ, 739, 38
Papastergis E., Giovanelli R., Haynes M. P., Shankar F., 2015, A&A, 574, A113
Planck Collaboration I, 2014, A&A, 571, A1
Polisensky E., Ricotti M., 2014, MNRAS, 437, 2922
Reed D. S., Bower R., Frenk C. S., Jenkins A., Theuns T., 2007, MNRAS, 374, 2
Salvadori S., Ferrara A., 2012, MNRAS, 421, L29
Sawala T. et al., 2016, MNRAS, 456, 85
Sawala T. et al., 2015, MNRAS, 448, 2941
Shapiro P. R., Iliev I. T., Raga A. C., 2004, MNRAS, 348, 753
Shimasaku K., 1993, ApJ, 413, 59
Springel V. et al., 2005, Nature, 435, 629
Springel V. et al., 2008, MNRAS, 391, 1685
Starkenburg E. et al., 2013, MNRAS, 429, 725
Trujillo-Gomez S., Klypin A., Primack J., Romanowsky A. J., 2011, ApJ, 742, 16
Vera-Ciro C. A., Helmi A., Starkenburg E., Breddels M. A., 2013, MNRAS, 428, 1696
Vogelsberger M., Zavala J., Simpson C., Jenkins A., 2014, MNRAS, 444, 3684
Zavala J., Jing Y. P., Faltenbacher A., Yepes G., Hoffman Y., Gottlöber S., Catinella B., 2009, ApJ, 700, 1779

This paper has been typeset from a TEX/LATEX file prepared by the author.